On the effect of distributed cooling in natural ventilation

S. R. LIVERMORE AND A. W. WOODS

BP Institute for Multiphase flow, University of Cambridge, Cambridge, CB3 0EZ, UK

We examine the natural ventilation flows which develop when a low-level heat source interacts with a distributed zone of cooling at high level in an enclosed space. We develop some new analogue laboratory experiments in which we use a saline plume to model a localized heat source and a heated plate to model a distributed source of cooling. The experiments show that in a building with a low-level point source of heating, a two-layer steady stratification develops in which the depth of the lower layer decreases as the intensity of the cooling at the ceiling increases. We develop a theoretical model which accounts for the penetrative entrainment across the interface associated with the convection in the upper layer. We show that this becomes more dominant as the cooling increases and eventually the room becomes well-mixed. We discuss the role of such distributed cooling on the design of natural ventilation and its ability to provide sufficient flow and adequate temperature control.

1. Introduction

Much of the recent interest in the fluid mechanics of natural ventilation has focused on upward buoyancy-driven flows produced by heat loads within a space which act to heat the air (Linden 1999). However, heat loads within a building can lead to heating of the building fabric, through both radiative and convective heat exchange. This can then lead to the walls and ceiling of a building acting as heat sources or sinks for the internal air (Fisk 1981; Sandberg & Lindstrom 1990; Davies 2004). Similarly, in poorly insulated buildings, heat conduction through the walls and roof can cool the building mass in winter, and this in turn acts as a heat sink for the air. Typically the thermal mass of a building has a heat capacity of 10–100 times that of the air owing to the large contrast in density between the building material and air. As a result, the time scale for the temperature of the thermal mass to evolve, through radiative and convective heat transfer, is also 10–100 times longer than that of the air (Fisk 1981; Li & Yam 2004). This can lead to a phase lag between the temperature of the internal air and that of the building mass, in response to changes in the internal heat loads or the ventilation rate. This can then lead to significant convective heat exchange between the air and the mass of the building.

In typical cases, buildings have air change rates of 3–4 changes per hour, and hence establish quasi-steady convective flows within several tens of minutes. In contrast, the thermal mass typically has a time constant of a few hours (Fisk 1981; Davies 2004). Therefore, in modelling the quasi-steady natural convective flows within a building, we can assume that the thermal mass of the building has an approximately constant temperature, but that this evolves over a longer time scale in response to changes in the heat load, ventilation rate or the external temperature. In this limit,
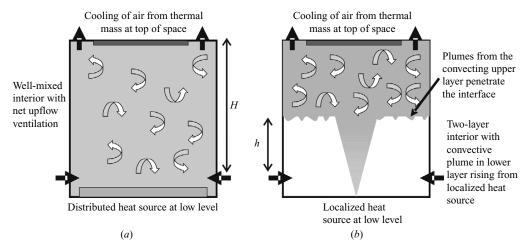
FIGURE 1. Schematic of the upward displacement ventilation flow which develops with a uniform source of cooling at the ceiling and (*a*) a distributed source of heating at the base of the room, and (*b*) a localized source of heating at the base of the room.

it is appropriate to model the convective heat transfer as being driven by a series of convective heat sources, associated with the activity in the building, and a series of heat sinks associated with the thermal mass (cf. Li & Yam 2004)

Our work is also relevant to situations in which there are mechanically chilled ceilings which are designed provide cooling in combination with displacement ventilation (Novoselac & Srebric 2002). The cold ceiling generates convective flow in the upper warm layer, which can again interact with the convective flows produced by heat sources lower in the space.

The purpose of the present work is to gain insight into how the structure and intensity of buoyancy-driven ventilation flows are affected by the combination of heat loads and heat sinks. In order to illustrate the key points, we consider a large aspect ratio building, such as an open plan office, in which the lateral extent of the space far exceeds the floor–ceiling height. In this case, the interior natural ventilation flows may be dominated by the convection associated with heat sources at low level and the distributed heat sink associated with thermal mass of the ceiling (figure 1). It is useful to consider two end-member models. First, the case of a distributed source of heating at low level, as occurs in an auditorium or other densely packed space (figure 1*a*). Then, we examine the case of localized heat convective sources, associated with radiators or highly energy intensive office equipment, such as printers (figure 1*b*).

The analysis of a distributed heat source follows from the work of Gladstone & Woods (2001), and we describe this below. The case of a localized heat source is more complex, and forms the topic of the remainder of the paper. We build from the pioneering work of Linden, Lane-Serff & Smeed (1990) who examined the case of a pure heat source and showed that a two-layer stratification becomes established. We develop a new model which accounts for the cooling-induced convection in the upper layer and test the predictions of this model with a series of new laboratory experiments. These experiments illustrate the importance of the penetrative entrainment of lower-layer fluid into the upper layer, especially when the strength of the convective cooling at the ceiling is comparable to the strength of the low-level convective heat source. We conclude with a discussion of the relevance of the work in real building applications.

2. Interaction of distributed heating and distributed cooling

In the idealized case of high Rayleigh number convection in a room which has a distributed source of heating at the floor, Q_h, and a distributed source of cooling at the ceiling, Q_c, the air in the room becomes well-mixed (figure 1a) and the steady-state natural ventilation has volume flux, V, given by Gladstone & Woods (2001),

$$V = \frac{Q_h - Q_c}{\rho C_p \Delta T}, \tag{2.1}$$

where the temperature in the room is ΔT warmer than the external temperature, T_e, and ρ and C_p are the density and specific heat of the air. The natural ventilation flow is given by Linden (1999):

$$V = cA^* \left(\frac{\Delta \rho g H}{\rho} \right)^{1/2}, \tag{2.2}$$

where c is the loss coefficient of the openings, A^* is the effective area of the openings, H is the vertical distance between the inflow and outflow vents and $\Delta \rho$, the density contrast with the exterior air, is

$$\Delta \rho = \rho \alpha \Delta T, \tag{2.3}$$

where α is the thermal expansion coefficient of the air. Combining the relations we find that the temperature excess in the room is given in terms of the net heat load (cf. Gladstone & Woods 2001)

$$\Delta T = \left(\left(\frac{Q_h - Q_c}{\rho C_p c A^*} \right)^2 \frac{1}{\alpha g H} \right)^{1/3} \tag{2.4}$$

and the ventilation flow then follows from (2.1). Equation (2.4) is useful as it identifies the reference temperature scale,

$$\Delta T_o = \left(\left(\frac{Q_h}{\rho C_p c A^*} \right)^2 \frac{1}{\alpha g H} \right)^{1/3}, \tag{2.5}$$

which corresponds to the case in which there is no ceiling cooling, and all the convective heating is ventilated from the space.

3. Modelling the interaction of localized heating with distributed cooling

Linden *et al.* (1990) showed that with upward displacement ventilation, a localized source of heating leads to a two-layer stratification in which a warm layer of heated air overlies a layer of cool external air. When there is a distributed source of cooling at the ceiling, the upper layer transfers heat to the ceiling and therefore the overall energy balance changes. This leads to a change in the depth and temperature of the upper layer, as well as the ventilation rate. We now explore the fluid mechanics of this new regime using a simple theoretical model and some supporting analogue laboratory experiments (figure 1b).

When a room is heated by a localized convective heat source, Q_p, located at the base of the room, a turbulent convective plume develops and carries heat to the top of the room. This warm air vents from the upper opening, and we expect a two-layer stratification to develop, with the lower layer being composed of cool external air and the upper warm layer arising from the volume flux of warm air supplied by the

convective plume, V_p, say. However, the upper layer will also be in a state of turbulent convection owing to the cooling at the ceiling, and this leads to turbulent penetrative convection at the interface with the cold air, and an associated flux V_c of lower layer air into the upper layer. The overall upward displacement ventilation, with volume flux V, matches these two volume fluxes:

$$V = V_c + V_p. \tag{3.1}$$

Similarly, the overall convective heat balance in the room matches the convective heat source, Q_p, with the convective heat sink at the ceiling, Q_c, and the convective heat loss associated with the ventilation, leading to the expression

$$Q_p = Q_c + \rho C_p \Delta T V, \tag{3.2}$$

where ΔT is the temperature excess of the air in the upper layer relative to the exterior.

The volume flux V_p can be estimated using the classical theory of turbulent buoyant plumes (Morton, Taylor & Turner 1956):

$$V_p = \lambda B_p^{1/3} h^{5/3}, \tag{3.3}$$

where λ is the integrated entrainment constant as described in the analysis of the experiments (§4.2). Also, here h is the depth of the lower layer of cool external air, and

$$B_p = g\alpha Q_p / \rho C_p \tag{3.4}$$

is the buoyancy flux associated with the heat source Q_p. The overall upward displacement ventilation flow is given by (Linden 1999)

$$V = cA^* \left(g\alpha \Delta T (H - h) \right)^{1/2}, \tag{3.5}$$

where α is the thermal expansion coefficient of the fluid. Finally, we model the rate of entrainment of lower-layer fluid V_c driven by the roof cooling and associated turbulent convection in the upper layer. As eddies descending through the upper layer impinge on the interface and penetrate into the lower layer, some of the lower-layer fluid may be entrained and mixed into the upper layer. The movement of fluid from the lower to the upper layer depends on the intensity of the turbulent motions and also on the density contrast between the fluid in each layer. Numerous experimental and theoretical studies of penetrative convection aimed at quantifying the rate of mixing across the interface have been described in the literature (Zilitinkevich 1991; Deardorff, Willis & Lilly 1969; Denton & Wood 1981; Lister 1995). Many such studies have described the rate of entrainment in terms of the local Richardson number at the interface. However, for high Péclet number convection in the upper layer, Zilitinkevich (1991) has proposed that for a distributed source of cooling, the rate of entrainment across the interface may be expressed in terms of the fraction ϕ of the buoyancy released at the cooled boundary, B_c, which is used to generate buoyancy through entrainment across the interface:

$$V_c = \phi B_c / g'_u, \tag{3.6}$$

where

$$g'_u = g\Delta\rho_u / \rho = g\alpha\Delta T, \tag{3.7}$$

with subscript u denoting the upper layer. The buoyancy flux associated with the heat exchange at the ceiling, Q_c, is denoted by

$$B_c = g\alpha Q_c/\rho C_p. \tag{3.8}$$

A number of experimental studies suggest that ϕ has a value of order 0.2 ± 0.1 (Zilitinkevich 1991). We adopt and test this model herein.

To illustrate the impact of the roof cooling and the penetrative convection, it is convenient to introduce the dimensionless ratio $\hat{Q}$ of the rate of roof cooling to the plume heating

$$\hat{Q} = Q_c/Q_p \tag{3.9}$$

and the dimensionless depth of the interface

$$\zeta = h/H. \tag{3.10}$$

Then combining the above model equations (3.1)–(3.10), it is possible to show that

$$\zeta^5 = \Gamma(1-\zeta)\frac{[1-\hat{Q}(1+\phi)]^3}{(1-\hat{Q})^2}, \tag{3.11}$$

where

$$\Gamma = c^2 A^{*2}/(H^4\lambda^3) \tag{3.12}$$

is a constant. In the limit $\hat{Q}=0$ there is no cooling at the ceiling and we recover the model of Linden *et al.* (1990). However, in the limit $\hat{Q} \to 1/(1+\phi)$ the depth of the lower layer approaches zero, and the whole room is predicted to become well-mixed. However, as $\hat{Q}$ increases towards this value, as we will see in the experiments, we expect the penetrative convection to become more intense, and the interface less well-defined, so that the present model becomes somewhat too simplified to describe the mixing and flow. The variation of the interface height with $\hat{Q}$ as predicted by the model is shown in figure 2(*a*). The dimensionless temperature $\theta = (T - T_e)/\Delta T_o$, which is related to the buoyancy by the relation $g_u' = g\alpha\theta\Delta T_o$, where ΔT_o is defined by (2.5), is given by

$$\theta = \left(\frac{(1-\hat{Q})^2}{1-\zeta}\right)^{1/3}. \tag{3.13}$$

Again, this reduces to the limit of Linden *et al.* (1990) in the limit $\hat{Q}=0$, but as the heat flux at the ceiling intensifies, the lower layer becomes progressively shallower, and the upper-layer temperature falls, as shown in figure 2(*b*). In figure 2, curves are given for $\Gamma = 0.1$, and 0.01 which correspond to the approximate values for the ratio of the opening area to the square of the depth of the room $A/H^2 \sim 0.04$ and 0.004.

4. Experimental study of distributed roof cooling and localized floor heating

We have developed an analogue laboratory experiment to test the predictions of the model of §3 in which a localized source of heating is coupled with a distributed source of cooling. In our experiments, we use a small-scale water bath as an analogue for flow of air in a building. Using the principles of dynamic similarity (Linden 1999; Gladstone & Woods 2001), these experiments can replicate the large-scale features of air flow in buildings provided the Reynolds numbers of air flow through openings,
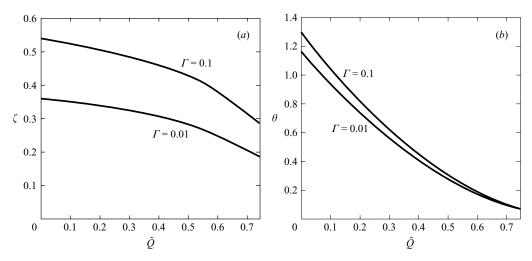
FIGURE 2. (a) Variation of the depth of the lower layer of external air, and hence of the interface with the upper warm layer, as a function of the ratio of the cooling load at the ceiling to the heating load at the base of the room, $\hat{Q}$. Curves are given for $\Gamma = 0.01, 0.1$. (b) Variation of the depth of the upper-layer temperature as a function of $\hat{Q}$. Curves are again given for two values of Γ.

and the Rayleigh and Péclet numbers of the convection are sufficiently large. To this end we use a small-scale model building of dimensions $20 \times 20 \times 40$ cm, immersed in a large reservoir tank.

For experimental convenience, we decided to model the distributed source of cooling at the ceiling of the room with a distributed source of heating on the floor of the experimental tank, and we model the localized source of convective heating at the floor of the room, with a localized source of dense saline water at the top of the tank (figure 3). This allowed us to combine two experimental systems available in the BP institute the hot-wire system, as described by Gladstone & Woods (2001), which has been shown to be an effective means of producing a distributed heat source, and the buoyant-plume apparatus, as described by Woods, Caulfield & Phillips (2003), which is a well-established means of generating a turbulent buoyant plume from a localized source of buoyancy (see Morton et al. 1956; Turner 1979). Using this experimental system, we can control the analogue of the ceiling cooling load, B_c, by measuring the power supply to the high-resistance wire and then calculate the effective buoyancy flux of this heat source using (3.8). Similarly, we can estimate the effective buoyancy flux of the saline plume, B_p, which models the localized heat source, by calculating the product of the buoyancy and volume flow, V_s, of the saline fluid supplied to the plume source:

$$B_p = g\beta \Delta S V_s, \tag{4.1}$$

where β is the relative rate of change of density with salinity and ΔS is the salinity difference between the plume fluid and the ambient reservoir fluid. In our work, we have measured salinity as the mass fraction in solution, and using this definition and measurements of density of the aqueous solutions, we find that $\beta \sim 0.007$ for the range of salinities used in our experiments. By working with these buoyancy fluxes, we can compare the effect of the heating load and the saline plume on the flow pattern, and then test the predictions of the model presented in §3.
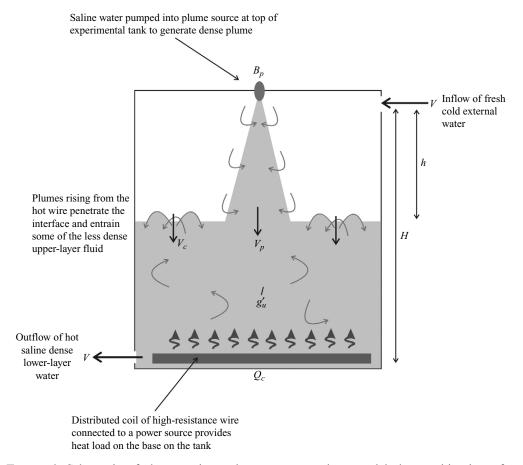
Saline water pumped into plume source at top of
experimental tank to generate dense plume

Plumes rising from the
hot wire penetrate the
interface and entrain
some of the less dense
upper-layer fluid

Outflow of hot
saline dense
lower-layer
water

Distributed coil of high-resistance wire
connected to a power source provides
heat load on the base on the tank

Inflow of fresh
cold external
water

FIGURE 3. Schematic of the experimental apparatus used to model the combination of a localized source of heating at the base of the room and a distributed source of cooling at the top of the room.

In our experiments, the flow is of high Reynolds number, and hence the transport of heat and salt are dominated by turbulent convective fluxes. Indeed, the penetrative convection which occurs at the interface is driven by the heating at the base of the tank which drives plumes up through the interface. These plumes entrain fluid from the relatively fresh, but cool, layer of ambient fluid (which is the overlying layer in the experiment). Since the Péclet number of the thermal convection in the buoyant layer (which is the lower layer in the experiment) is high, we expect the mixing of the layer of ambient fluid (the upper layer in the experiment) into the buoyant layer of relatively saline and warm fluid (the lower layer in the experiment) by these penetrating plumes to be controlled by the buoyancy flux at the base of the tank, and the buoyancy contrast across the interface (see Deardorff *et al.* 1969; Zilitinkevich 1991). Therefore, for the purposes of the present steady-state modelling, our experimental model provides a satisfactory analogue of the purely thermal convection which occurs in a building. However, care needs to be taken in extending the modelling to other flow situations, such as the transient non-ventilated flow regime, in which double-diffusive effects may influence or even dominate the results (see McDougall 1983).

4.1. *Methodology*

We conducted a series of experiments to explore the effect of the heating at the base of the tank on the downward displacement ventilation produced by the descending saline plume.

For the purpose of modelling the experiments, we first carried out a series of calibration experiments to determine the integrated entrainment coefficient λ for the plume source used in the experiments (equation (3.3)), and then we tested the model in the limit of a pure saline plume with no heat load. Finally, we included the effect of heating to explore the interaction between the localized and distributed sources of buoyancy.

4.2. *Calibration experiments*

To calibrate the plume source we followed the approach of Baines (1983) and imposed a ventilation flow at the base of the experimental tank by extracting a known flux of fluid from the base of the tank through a peristaltic pump. We then supplied a known buoyancy flux through the plume source and systematically varied the ventilation rate, measuring the steady-state interface height, h, for each flow rate. According to the classical theory of turbulent buoyant plumes (Morton *et al.* 1956; §3), the volume flux $V_p(h)$ in the plume varies as

$$V_p(h) = \lambda B_p^{1/3}(h + z_o)^{5/3}, \tag{4.2}$$

where the virtual origin, z_o can be estimated in terms of the volume flux at the source, V_s, according to

$$V_s = \lambda B_p^{1/3} z_o^{5/3}. \tag{4.3}$$

By comparing the imposed ventilation flow with the theoretical plume flux based on the experimentally observed height of the interface, we can thereby estimate λ. The range of values of λ from these experiments is shown in figure 4. Experiments were conducted using three buoyancy fluxes; 3% salt solution with a plume flux of $0.7\,\mathrm{cm^3\,s^{-1}}$ 5% solution with $1\,\mathrm{cm^3\,s^{-1}}$ and 10% solution with $0.7\,\mathrm{cm^3\,s^{-1}}$ which gave buoyancy fluxes of $1.6 \times 10^{-7}\,\mathrm{m^4\,s^{-3}}$ (crosses), $3.8 \times 10^{-7}\,\mathrm{m^4\,s^{-3}}$ (dots) and $5.3 \times 10^{-7}\,\mathrm{m^4\,s^{-3}}$ (diamonds) respectively. The forced ventilation from the dense lower layer was varied between $12\,\mathrm{cm^3\,s^{-1}}$ and $80\,\mathrm{cm^3\,s^{-1}}$. Figure 4 shows that the data lie in the range 0.2 ± 0.02. It is this empirically determined value of λ, emerging from these calibration experiments, which we take forward in the subsequent modelling. For comparison with earlier work, the entrainment parameter λ is related to the so-called top-hat entrainment coefficient α (see Turner 1979) according to the relation $\lambda = (6\alpha/5)(9\alpha\pi^2/10)^{1/3}$. Numerous independent experiments have found $\alpha/\sqrt{2} \sim 0.1 \pm 0.01$ (e.g. Turner 1979; Baines 1975). The present experimental measurement $\lambda \sim 0.2$ is equivalent to the value $\alpha/\sqrt{2} = 0.107$. Also, in the experiments, we found that the virtual origin had the value $10 \pm 2\,\mathrm{mm}$. We note that in the experiments reported in this paper the volume flow supplied with the source of buoyancy is only 1–5% of the ventilation flow so that the effects of the finite source mass flux are unimportant (see Woods *et al.* 2003).

We then conducted a series of experiments in which the saline plume produced the classical downward displacement ventilation flow as described by Linden *et al.* (1990). If we allow for a virtual origin in the model of §3, then the height of the interface is given by (cf. (3.11))

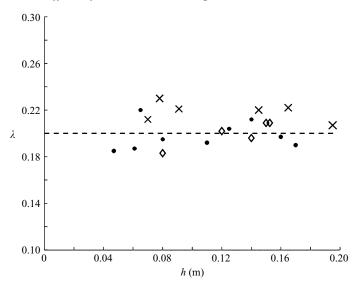$$\left(\zeta + \frac{z_o}{H}\right)^5 = \Gamma(1 - \zeta). \tag{4.4}$$

FIGURE 4. Variation of the value of λ, the entrainment coefficient, as measured in a series of experiments in which there was a forced ventilation flow and the height of the interface was measured to estimate the value of λ from the classical plume theory. Three values of the buoyancy flux were used, $1.6 \times 10^{-7} \, \mathrm{m^4 \, s^{-3}}$ (crosses), $3.8 \times 10^{-7} \, \mathrm{m^4 \, s^{-3}}$ (dots), $5.3 \times 10^{-7} \, \mathrm{m^4 \, s^{-3}}$ (diamonds) and the ventilation was varied between $12 \, \mathrm{cm^3 \, s^{-1}}$ and $80 \, \mathrm{cm^3 \, s^{-1}}$ in steps of approximately $0.2 \, \mathrm{cm^3 \, s^{-1}}$.
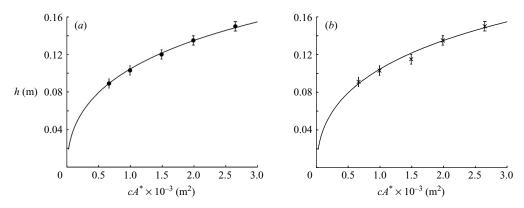

FIGURE 5. Variation of the height of the interface as a function of the magnitude of the effective opening area of the room for a buoyancy flux (a) $B_p = 1.5 \times 10^{-7} \, \mathrm{m^4 \, s^{-3}}$ and (b) $B_p = 2.5 \times 10^{-7} \, \mathrm{m^4 \, s^{-3}}$. The experimental data from the salt-bath analogue experiments (symbols) are compared with the theoretical model (solid and dashed lines) based on Linden *et al.* (1990) using the entrainment coefficient as determined from figure 4.

Figure 5 compares the prediction of the interface height as a function of cA^*, the effective area of the opening, for two buoyancy fluxes (a) $1.5 \times 10^{-7} \, \mathrm{m^4 \, s^{-3}}$ (using 3 % solution with $0.7 \, \mathrm{cm^3 \, s^{-1}}$ flux) and (b) $2.5 \times 10^{-7} \, \mathrm{m^4 \, s^{-3}}$ (5 % solution with $0.7 \, \mathrm{cm^3 \, s^{-1}}$ flux). Equation (3.13) relates cA^* to Γ. The agreement of the data with the model is good. This is relevant since, in our experiments, the lateral dimensions of the tank are comparable to the height of the tank. Therefore, it would be possible for wall currents to develop and enhance the mixing in the interior if a strongly buoyant plume impinged on the floor of the tank and spread to the walls. However, the good

agreement of the emptying–filling box model of Linden *et al.* (1990), which neglects the effects of any wall currents, with our calibration experiments (figure 5) suggests that wall currents are of secondary importance in our experiments.

4.3. *Results of combined heating and cooling*

Given the calibration of the experimental system, the only free parameter in the model described in §3 is the coefficient ϕ which quantifies the efficiency of the penetrative convection. Previous experimental studies suggest that $\phi = 0.2 \pm 0.1$ (Zilitinkevich 1991; Cardoso & Woods 1996). We now compare the predictions of this model with our new experiments in which there is a distributed heat source at the base of the tank and a localized source of dense saline fluid at the top of the tank. In our experiments, we fixed the buoyancy flux associated with the plume of saline fluid, and then systematically varied the strength of the heat source at the base of the tank. As the heat source became more intense, the interface ascended further from the floor of the tank, owing to the reduction in the (negative) buoyancy of the lower layer associated with the heating. Figure 6 illustrates a typical series of four experiments where the plume flux is $B_p = 1.6 \times 10^{-7} \, \mathrm{m^4 \, s^{-3}}$ (0.7 cm³ s⁻¹ flux with 3 % salinity) and $\Gamma = 0.18$. The heat load was increased through the range, 0, 100 W, 230 W and 350 W equating to $\hat{Q} = 0, 0.3, 0.7$ and 1 figures 6(*a*)–6(*d*) respectively. In each case there is a well-defined interface between the red lower layer of plume fluid and the clear layer of external fluid entering the tank from above (the upper layer in the experiment). As the heating increases for a fixed plume-buoyancy flux, the interface deepens, but also becomes more irregular and subject to more vigorous plume entrainment events. In figure 7 we illustrate this trend by plotting the depth of the ambient layer (the upper layer in the experiment), which represents the distance of the interface from the top of the tank, as a function of the ratio of buoyancy flux associated with the distributed heating compared to that of the saline plume source. This ratio corresponds to the parameter $\hat{Q}$, in the model of §3 which defines the heat loss from the ceiling to the localized heat gain to the room at low level. We plot data for two sizes of ventilation areas, $\Gamma = 0.1$ (figure 7*a*) and $\Gamma = 0.18$ (figure 7*b*). In addition we use the two plume-buoyancy fluxes of §4.2, $1.5 \times 10^{-7} \, \mathrm{m^4 \, s^{-1}}$ (dots) and $2.5 \times 10^{-7} \, \mathrm{m^4 \, s^{-3}}$ (crosses) and vary the distributed heating such that $0 < \hat{Q} < 1$. When the parameter $\hat{Q}$ reaches a magnitude in excess of about 0.6–0.7, the interface becomes very undular. Plumes overshoot the interface and approach the top of the tank, so that the system does not have a well-defined interface, but instead it approaches a well-mixed regime.

Figure 7 also illustrates the predictions of the theoretical model, using values $\phi = 0$ (solid line), 0.1, 0.14 and 0.2 (dotted lines). The model with $\phi = 0$ does not represent the data very accurately, and emphasizes the importance of the penetrative convection on the process of mixing. Although not a perfect fit, within the experimental error, the data for $0 < \hat{Q} < 0.7$ are reasonably well modelled with a value $\phi \sim 0.14 \pm 0.05$, which is in accord with earlier literature on penetrative convection (Zilitinkevich 1991; Cardoso & Woods 1996). For larger values of $\hat{Q}$ when the convection becomes more intense, this simple one-dimensional description ceases to be sufficiently detailed to model the two-dimensional nature of the flow, with convective plumes penetrating high above the interface: although some data points have been shown for the mean location of the interface with $\hat{Q} > 0.7$, these are subject to large fluctuations associated with the plume motion. To describe the motion in that regime, as the flow evolves to the fully mixed regime, a more complete two-dimensional model of the eddy-driven mixing would be required.
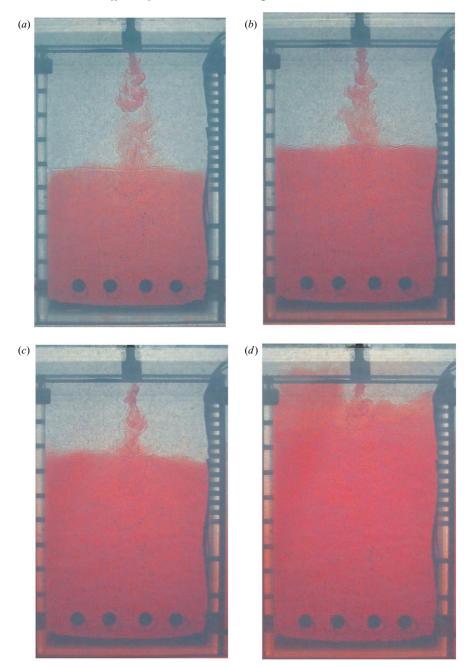
FIGURE 6. Series of photographs of four experiments in which there is a saline plume of constant flux, $B_p = 1.6 \times 10^{-7}\,\mathrm{m^4\,s^{-3}}$ and the magnitude of the heat load supplied to the distributed heating system is progressively increased: (*a*) 0, (*b*) 100 W, (*c*) 230 W and (*d*) 350 W equating to $\hat{Q} = 0$, 0.3, 0.7 and 1. We see that as this ratio increases, the depth of the buoyant layer of red dyed fluid (the lower layer in the experiment) increases, until eventually the room becomes well mixed.
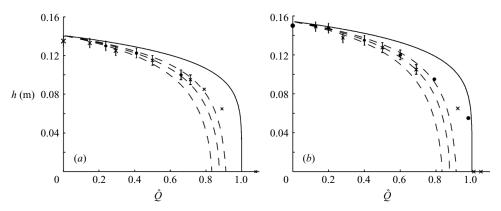
FIGURE 7. Variation of the depth of the buoyant layer (the lower layer in the experiment), and hence of the depth of the interface, as measured experimentally, shown as a function of the ratio $\hat{Q}$: in (a) $\Gamma = 0.1$ while in (b) $\Gamma = 0.18$. The theoretical curves correspond to the predictions of the model in the cases $\phi = 0$ (solid line), 0.1, 0.14 and 0.2 (dotted lines). The crosses indicate the the experimental data points for a plume of buoyancy flux, $B_p = 1.5 \times 10^{-7} \, \mathrm{m^4 \, s^{-3}}$ and the circles for $B_p = 2.5 \times 10^{-7} \, \mathrm{m^4 \, s^{-3}}$.

5. Discussion

The model and experiments presented in §§2–4 were based on the simplifying assumption that there is a convective heat load at the floor of the space and an independent convective heat sink at the ceiling. The evolution of the flow and stratification were then quantified in terms of the ratio of these two heat fluxes, as given by the parameter $\hat{Q}$. The convective heat source arises from a combination of the activity in the space, the lighting and the convective component of the heating. The convective cooling may be associated with the thermal mass, in which case the surface temperature evolves slowly over time, or it may arise from a mechanically chilled ceiling, in which case the cooling load may be controlled.

In the case of a thermally massive ceiling, the convective heat exchange with the ceiling mass depends on the balance between the conduction of heat through the ceiling material, the radiative flux at the ceiling surface and the temperature contrast between the ceiling surface and the air. As the thermal mass heats up over a period of a few hours, through both radiative and convective heating, the convective cooling it provides to the air will decrease. As a result, the temperature distribution and flow rate of the air also evolve with time. With a uniform distribution of heating at low level, the mean temperature of the space will increase, and as a result the ventilation rate also increases (§2). If the sources of heating are more localized, then as the cooling capacity of the ceiling decreases, the temperature of the hot upper layer will increase, along with the ventilation rate. In response, the depth of the lower layer will increase. In this way, the intensity of any thermal stratification will tend to build up with time (figure 2; §3).

In contrast if the cooling load at the ceiling is associated with a (mechanically) chilled ceiling, the cooling load can be adjusted according to the heat load (Novoselac & Srebric 2002). However, with a quasi-steady cooling load from the ceiling, the fluid mechanical principles controlling the penetrative convection below a chilled ceiling are analogous to those associated with thermal mass. We consider the case of a chilled ceiling later in the section.

We first extend the model to illustrate how the ratio $\hat{Q}$ of the convective cooling at the ceiling to the convective heating at the base of the space depends on the temperature of the thermal mass. Typically, the heat flux through that part of the thermal mass which is in good thermal contact with the air may be linearized to the form $\rho_s C_s u(T_m - T_s)$ per unit area (Li & Yam 2004; Holford & Woods 2007), where T_m and T_s are the characteristic temperatures of the effective thermal mass and the surface, u is an effective heat transfer coefficient across the thermal mass which depends on the thermal diffusivity and the thickness of the mass, $\sim 10^{-5}\,\mathrm{m\,s^{-1}}$, and ρ_s and C_s are the solid density and specific heat (Holford & Woods 2007). The convective heat flux associated with the air flow near the surface of the thermal mass may be parameterized in the form $\rho C_p h_a(T - T_s)$ per unit area, where h_a is the effective heat transfer coefficient and ρ and C_p are the specific heat and density of the air, while T is the temperature of the air. Although h_a may depend weakly on $T - T_s$, for the purposes of the present discussion, we assume it is constant. Indeed, we adopt the value $h_a = 0.0025\,\mathrm{m\,s^{-1}}$, following the CIBSE (1999) guide for typical convective heat transfer coefficients in a building, but noting the simplification in taking this number to be a constant. We then have the approximate balance

$$\rho C_p h_a(T - T_s) = \rho_s C_s u(T_s - T_m),\tag{5.1}$$

which leads to an expression for the convective heat transfer from the air to the thermal mass:

$$Q_c = \hat{u}(T - T_m),\tag{5.2}$$

where

$$\hat{u} = \frac{\rho C_p \rho_s C_s h_a u}{\rho C_p h_a + \rho_s C_s u}.\tag{5.3}$$

We now combine this relation with the models of §§2 and 3 to estimate how the temperature of the air and the ventilation rate depend on the temperature of the thermal mass. To proceed it is useful to work with the dimensionless temperature of the thermal mass, defined as

$$\theta_m = (T_m - T_e)/\Delta T_o,\tag{5.4}$$

where ΔT_o is the temperature of the air in the case of a distributed source of heating with no cooling at the ceiling (§2, (2.5)). We then set

$$\Omega = \hat{u}/\Delta T_o Q_h.\tag{5.5}$$

It follows that

$$\hat{Q} = \Omega(\theta - \theta_m).\tag{5.6}$$

For example, we apply the model to an open-plan working area with 100 people and a heat load of 18 kW. We estimate that $\hat{h} \sim 2$ and so $\Omega \sim 6$ in the case in which the ventilation flow is set to $3\,\mathrm{m^3\,s^{-1}}$, $\Delta T_o \sim 6\,°\mathrm{C}$, and the area of the space $A \sim 10^4\,\mathrm{m^2}$.

In the case of a well-mixed space, the model of §2 (equation (2.4)) leads to the relation

$$\theta = (1 - \Omega(\theta - \theta_m))^{2/3}.\tag{5.7}$$

In figure 8(a) we show how θ, the temperature of the air, and $\hat{Q}$, the ratio of the cooling at the ceiling to the heating at low level, depend on the dimensionless temperature of the thermal mass for the case of a distributed heat source. As the thermal mass heats up beyond the external temperature, $\theta_m = 0$, the ratio of cooling to heating gradually decreases, while the temperature of the air converges towards
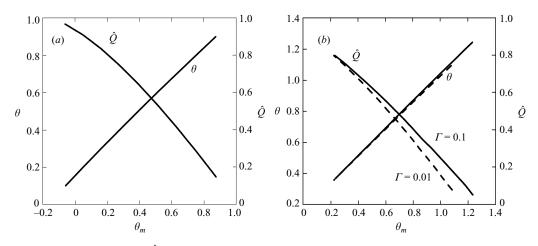
FIGURE 8. Variation of $\hat{Q}$, the fraction of the heat load from (*a*) a distributed and (*b*) a localized low-level source of heating, which is taken up by convective exchange with the ceiling, as a function of the temperature of the ceiling thermal mass, θ_m. The calculation is an upper bound in that we neglect the effects of radiative transfer to the ceiling, which will reduce the convective exchange; this limit is appropriate with localized low-temperature convective heat sources. In (*b*), curves are given for $\Gamma = 0.1$ and 0.01.

that of the thermal mass. In figure 8(*b*) we show the analogous plot for the case of a localized source of heating (cf. figure 2*b*), in which the parameter Γ as defined by (3.12) takes the values $\Gamma = 0.1$ and 0.01. The figure shows a similar trend. By reference to figure 2(*b*), we can also infer that as the thermal mass heats up and the heat transfer to the ceiling decreases, the depth of the lower layer increases and the upper layer heats up.

In applying the model to real applications, we note that typically there are a large number of sources of radiative heating which influence the surface temperature of the thermal mass. In developing a more complete thermal model of a building, and of the evolution of the temperature of the thermal mass, this radiant heat transfer is also important. The present model could therefore be coupled with a model of such radiant heat transfer to form a more complete model of the balance between convective and radiant heat transfer within a building.

We now turn to the case of a building with a chilled ceiling operating in a regime of upward displacement ventilation. Novoselac & Srebric (2002) reported numerous observations that with this configuration the interior air becomes vertically stratified. We now use the present model to provide some insight into the controls on the interface height and temperature of the upper layer. We suppose that in this controlled regime there is an upward ventilation rate V and that the incoming air is ΔT cooler than the air which vents from the top of the space. We also assume that the heat source at low-level Q_p arises from a localized low-level source, and forms a rising turbulent buoyant plume. Such a flow might develop due to the heat load associated with an occupant or some computing equipment. The cooling load, Q_c, which is assumed to be smaller than the heat load, Q_p, is controlled by the chilling system. In this case, (3.1) and (3.3) lead to the expression for the height (above the heat source) of the interface, h, given by

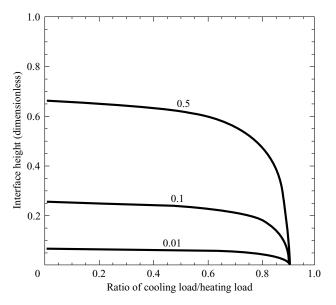$$V = \lambda B_p^{1/3} h^{5/3} + \frac{\phi Q_c}{\rho C_p \Delta T}, \qquad (5.8)$$

FIGURE 9. Variation of ζ, the height of the interface in an upflow displacement ventilation system with a chilled ceiling, as a function of the ratio of the cooling and the heating heat flux. The calculation is an upper bound in that we neglect the effects of cooling on the walls, and any radiative transfer. Curves are given for $\chi = 0.5$, 0.1 and 0.01.

where $B_p = (Q_p g \alpha / \rho C_p)$ while the temperature contrast across the interface is given by

$$\Delta T = \frac{Q_p - Q_c}{\rho C_p V}. \tag{5.9}$$

These expressions may be combined into a relation between the interface depth, $\zeta = h/H \leqslant 1$, and the relative strength of the cooling and heating, $\hat{Q} = Q_c/Q_p$, of the form

$$\zeta^{5/3} = \chi \left(1 - \phi \left(\frac{\hat{Q}}{1 - \hat{Q}} \right) \right), \tag{5.10}$$

where the parameter

$$\chi = \frac{V}{\lambda B_p^{1/3} H^{5/3}} \tag{5.11}$$

represents the ratio of the applied flow V and the plume volume flux at a height H above the source (equation 2.3).

We illustrate the predictions of this model in figure 9 in which we plot the model interface height as a function of the ratio of the cooling to heating load, taking $\phi = 0.1$ for the penetrative convection parameter (§4). Expressions (5.9) and (5.10) and figure 9 identify that if the cooling load increases, then the upper mixed layer deepens and cools. Indeed as $\hat{Q} \rightarrow 1/(1 + \phi)$, then $\zeta \rightarrow 0$, so that the upper mixed layer deepens towards the floor. Equations (5.9) and (5.10) and figure 9 also identify that as the ventilation flow and hence χ increases, the interface also rises, and the upper mixed layer becomes shallower and colder. Eventually, if the ventilation flow increases to a value comparable to the plume volume flux at the top of the room, $\chi \sim 1$, the interface also tends to rise towards to top of the room, $\zeta \rightarrow 1$. The convective component of the cooling is then of little value

since it only cools a shallow layer of air below the ceiling which vents from the space. However, any radiant cooling associated with the chilled ceiling does still operate.

As an example, let us consider an office type space with a floor to ceiling height of 4 m, and in which, over a 10 m² floor area, $V = 0.04\,\text{m}^3\,\text{s}^{-1}$ and there is a localized low-level heat load $Q_p = 300\,\text{W}$ and a total cooling load of 200 W in the ceiling. In this case, $\chi \sim 0.04$, while $\hat{Q} = 0.66$ and our model predicts $\zeta \sim 0.13$. This corresponds to the interface being about 0.4 m above the heat source.

6. Conclusions

This work has examined the impact of convective heat exchange with a thermally massive ceiling or a chilled ceiling on natural buoyancy-driven displacement ventilation. With a distributed heat source, we find that, as the convective heat transfer to the building mass increases, both the temperature of the interior air and the ventilation flow through the space are reduced.

We also find that when the heat source is localized, a two-layer stratification forms within the space, as in the case with no convective heat exchange at high level (Linden *et al.* 1990). However, with natural ventilation, the heat loss from the upper layer through convective exchange with the ceiling leads to a deeper cooler upper layer, and a smaller ventilation flow. This deepening is in part a result of penetrative convection whereby descending plumes in the upper convecting layer of fluid entrain some of the cool lower-layer fluid. As a progressively larger fraction of the heat source supplied at the base of the room is exchanged with the cold ceiling, the upper layer deepens and eventually reaches the floor, so the room becomes essentially well mixed.

We have developed a new analogue experimental model to investigate the interaction of a localized low-level heat source, and a high-level distributed source of cooling, using a combination of a high-resistance wire, which produces a distributed heat source, and a localized saline plume. The experimental results are in good accord with our theoretical predictions, and enable us to quantify the intensity of the penetrative convection, following the approach of Zilitinkevich (1991).

Our results suggest that as the thermal mass is gradually heated up through the convective exchange from the warm upper layer the fraction of the heat load which is transferred to the ceiling falls, and so the effective convective heat load driving the ventilation increases. This leads to progressively higher ventilation rates, and, with a localized heat source, the room becomes more strongly stratified.

Our results are also of interest for the interior stratification in an open-plan area with a mechanical chilled ceiling system, upflow displacement ventilation and a localized source of heating. If the ventilation rate is fixed, then as the cooling load at the ceiling is increased, our model shows that the upper layer becomes cooler and deeper. If the ventilation rate is increased, our model shows that the upper layer becomes cooler but shallower. These different responses of the system provide some insights into the control of such upward displacement, chilled ceiling systems.

REFERENCES

BAINES, W. D. 1975 Entrainment by a plume or jet at a density interface. *J. Fluid Mech.* **68**, 309–320.

BAINES, W. D. 1983 A technique for the measurement of volume flux in a plume. *J. Fluid Mech.* **132**, 247–256.

CARDOSO, S. S. S. & WOODS, A. W. 1996 Interfacial turbulent mixing in stratified magma reservoir. *J. Volcanolo. Geotherm. Res.* **73**, 157–175.

CIBSE 1999 *Environmental Design*. CIBSE Guide A, London.

DAVIES, M. G. 2004 *Building Heat Transfer*. Wiley.

DEARDORFF, J. W., WILLIS, G. E. & LILLY, D. K. 1969 Laboratory investigation of non-steady penetrative convection. *J. Fluid Mech.* **35**, 7–31.

DENTON, R. A. & WOOD, I. R. 1981 Penetrative convection at low peclet number. *J. Fluid Mech.* **111**, 1–21.

FISK, D. J. 1981 *Thermal Control of Buildings*. Applied Science.

GLADSTONE, C. & WOODS, A. W. 2001 On buoyancy-driven natural ventilation of a room with a heated floor. *J. Fluid Mech.* **441**, 293–314.

HOLFORD, J. & WOODS, A. W. 2007 The role of thermal mass in natural ventilation. *J. Fluid Mech.* **580**, 3–29.

LI, Y. & YAM, J. C. W. 2004 Designing thermal mass in naturally ventilated buildings. *Intl J. Ventilation* **2**, 313–324.

LINDEN, P. F. 1999 The fluid mechanics of natural ventilation. *Annu. Rev. Fluid Mech.* **31**, 201–238.

LINDEN, P. F., LANE-SERFF, G. F. & SMEED, D. A. 1990 Emptying filling boxes: the fluid mechanics of natural ventilation. *J. Fluid Mech.* **212**, 300–335.

LISTER, J. A. 1995 On penetrative convection at low peclet number. *J. Fluid Mech.* **292**, 229–248.

MCDOUGALL, T. J. 1983 Double-diffusive plumes in unconfined and confined environments. *J. Fluid Mech.* **133**, 321–343.

MORTON, B. R., TAYLOR, G. I. & TURNER, J. S. 1956 Turbulent gravitional convection from maintained and instantaneous sources. *Proc. R. Soci. Lond* A **234**, 1–23.

NOVOSELAC, A. & SREBRIC, J. 2002 A critical review on the performance and design of combined cooled ceiling and displacement ventilation systems. *Energy and Buildings* **34**, 497–509.

SANDBERG, M. & LINDSTROM, S. 1990 Stratified flow in ventilated rooms- a model study. *Proc. RoomVent Conference, Oslo, Norway*.

TURNER, J. S. 1979 *Buoyancy Effects in Fluids*. Cambridge University Press.

WOODS, A. W., CAULFIELD, C. P. & PHILLIPS, J. C. 2003 Blocked natural ventilation: the effect of a source mass flux. *J. Fluid Mech.* **495**, 119–133.

ZILITINKEVICH, S. S. 1991 Turbulent penetrative convection. *Avebury Tech.* pp. 1–77.